Conformational Transitions in Cytidine Bulge-Containing Deoxytridecanucleotide Duplexes: Extra Cytidine Equilibrates between Looped Out (Low Temperature) and Stacked (Elevated Temperature) Conformations in Solution†

Matthew W. Kalnik,‡ David G. Norman,‡,§ Michael G. Zagorski,‡ Peter F. Swann,§ and Dinshaw J. Patel*,‡

Department of Biochemistry and Molecular Biophysics, College of Physicians and Surgeons, Columbia University, New York, New York 10032, and Courtauld Institute of Biochemistry, Middlesex Hospital Medical School, London, England W1P 7PN

Received April 8, 1988; Revised Manuscript Received July 14, 1988

ABSTRACT: High-resolution homonuclear and heteronuclear two-dimensional NMR studies have been carried out on the self-complementary d(C-C-G-*C*-G-A-A-T-T-C-C-G-G) duplex (designated GCG 13-mer) in aqueous solution. This sequence contains an extra cytidine located between residues G3 and G4 on each strand of the duplex. The exchangeable and nonexchangeable proton resonances have been assigned from an analysis of two-dimensional nuclear Overhauser enhancement (NOESY) and correlated (COSY and relay COSY) spectra for the GCG 13-mer duplex in H_2O and D_2O solution. The extra cytidine at the bulge site (designated CX) results in more pronounced changes in the NOE distance connectivities for the G3–*CX*–G4 segment centered about the CX residue compared to the C9–C10 segment on the partner strand opposite the CX residue for the GCG 13-mer duplex at 25 °C. The cross-peak intensities in the short mixing time NOESY spectrum also establish that all glycosidic torsion angles including that of CX are anti in the GCG 13-mer duplex at 25 °C. The observed chemical shift changes for the CX base protons and the G3pCX phosphorus resonance with temperature between 0 and 40 °C demonstrate a temperature-dependent conformational equilibrium in the premelting transition region. The NOE and chemical shift parameters establish that the predominant conformation at low temperature (0 °C) has the extra cytidine looped out of the helix with the flanking G3·C10 and G4·C9 base pairs stacked on each other. These results support conclusions based on earlier one-dimensional NMR studies of extra cytidine containing complementary duplexes in aqueous solution [Morden, K. M., Chu, Y. G., Martin, F. H., & Tinoco, I., Jr. (1983) *Biochemistry 22*, 5557–5563. Woodson, S. A., & Crothers, D. M. (1987) *Biochemistry 26*, 904–912]. By contrast, the chemical shift and NOE parameters demonstrate that the conformational equilibrium shifts toward a structure with a stacked extra cytidine on raising the temperature to 40 °C prior to the helix-coil melting transition. The most downfield shifted phosphorus resonance in the GCG 13-mer duplex has been assigned to the phosphate in the C2–G3 step, and this observation demonstrates that the perturbation in the phosphodiester backbone extends to regions removed from the (G3–CX–G4)·(C9–C10) bulge site.

Single-base bulges can result as a consequence of slippage in tracts of identical base pairs in a DNA helix. The extra base can either stack into the helix or loop out into solution, introducing either addition (+1) or deletion (−1) frame-shift mutations due to the misalignment of the parent and daughter strands during replication (Streisinger et al., 1966). Base-pair mismatches and single-base bulges in the stem of hairpin loops generated at imperfect palindromic sequences have also been implicated in an alternate mechanism of frame-shift mutation (Ripley, 1982; De Boer & Ripley, 1984). The importance of bulge sites as recognition elements has been established from structural studies of the intercalative drug ethidium, which binds approximately an order of magnitude more tightly to a bulged cytidine site than to duplex binding sites [Nelson & Tinoco, 1985; White & Draper, 1987; see also Williams and Goldberg (1988)]. This preferential binding of the intercalator and the resulting stabilization of the bulged structure increase the likelihood of frame-shift mutation upon replication.

Early optical and photochemical measurements on noncomplementary synthetic RNAs (Lomant & Fresco, 1973) and DNAs (Evans & Morgan, 1982, 1986) have established that extra pyrimidines are looped out into solution. A more detailed characterization of the conformation of extra pyrimidines has required studies on DNA (Morden et al., 1983; Woodson & Crothers, 1987) and RNA (White & Draper, 1987) at the oligonucleotide level. Specifically, an NMR chemical shift and nuclear Overhauser enhancement (NOE) study on a deoxyoligonucleotide duplex containing an extra cytidine flanked by adenosines demonstrated that the extra cytidine loops out into solution and the flanking base pairs stack on each other (Morden et al., 1983). An extension of this research reported on NMR imino proton hydrogen exchange kinetics of deoxyoligonucleotide duplexes containing an extra base in a mutational hot spot sequence in the λC_1 gene (Woodson & Crothers, 1987). These workers established migration of an extra cytidine bulge over a range of flanking G·C base pairs in a homooligomeric segment.

By contrast, NMR chemical shift studies have established that an extra adenosine stacks into deoxyoligonucleotide duplexes (Patel et al., 1982), and this conclusion was confirmed by distance geometry analysis of distance constraints as deduced from two-dimensional NOESY data sets (Hare et al., 1986). These conflicting conclusions, that the extra adenosine stacks into the helix (Patel et al., 1982) while the extra cytidine loops out into solution (Morden et al., 1983), may reflect the contribution of the extra base (purine or pyrimidine) or the

† The research was supported by NIH Grant GM34504. The NMR spectrometers were purchased from funds donated by the Robert Woods Johnson, Jr., Trust and Matheson Trust toward setting up an NMR Center in the Basic Medical Sciences at Columbia University.

‡ Columbia University.

§ Courtauld Institute of Biochemistry.

0006-2960/89/0428-0294$01.50/0

flanking sequences on the stability of the helix at the interruption site.

A very interesting set of NMR experiments have been recently reported on pyrimidine bulge-containing duplexes containing identical deoxyoligonucleotide and ribooligonucleotide sequences (van der Hoogen et al., 1988a,b). The research demonstrated that the extra thymidine in the DNA duplex was stacked into the helix (van den Hoogen et al., 1988a), while the extra uridine in the identical RNA duplex was looped out into solution (van den Hoogen et al., 1988b).

We report on two-dimensional NMR studies of the self-complementary d(C-C-G-*C*-G-A-A-T-T-C-C-G-G) tridecanucleotide duplex (GCG 13-mer, Scheme I) that contains symmetrically related extra cytidines flanked by guanosines. Our efforts have focused on the conformation of the extra cytidine as a function of temperature in the duplex state.

Experimental Procedures

Oligonucleotide Synthesis. The oligodeoxyribonucleoside d(C-C-G-*C*-G-A-A-T-T-C-C-G-G) was synthesized by the solution-phase phosphotriester approach (Li et al., 1986) and deprotected by treatment with 1,1,2,2-tetramethylguanidinium *syn*-2-nitrobenzaldoximate (Reese & Zard, 1981), concentrated aqueous ammonia, and finally acetic acid/water. Purification of the deprotected DNA was by ion-exchange HPLC using a Partisil SAX column followed by desalting on a column of Sephadex G-25. The purified GCG 13-mer exhibits a retention time of 18.5 min on an analytical reverse-phase C18 column when eluted with a 0–30% gradient of acetonitrile over 30 min at 1 mL/min in 0.1 M triethylammonium acetate buffer. The oligomer was finally converted to the sodium form by passage through a short column of Dowex 50-X8 sodium form cation-exchange resin and then lyophilized.

Sample Preparation. The NMR spectra were recorded on 250 or 500 A_{260} units of GCG 13-mer duplex in 0.40 mL of 0.1 M NaCl, 10 mM phosphate, and 1 mM EDTA solutions with either 100% D_2O at pH 6.4 or 90% H_2O/10% D_2O (v/v) at pH 6.0 and 6.7. The pH values in D_2O are uncorrected pH readings.

NMR Experiments. One- and two-dimensional proton data sets on the GCG 13-mer duplex were collected on Bruker AM 400 and AM 500 spectrometers. Proton chemical shifts are referenced relative to internal TSP. One- and two-dimensional 121.5-MHz phosphorus data sets on the GCG 13-mer were collected on a Bruker AM 300 spectrometer. Phosphorus chemical shifts are referenced relative to internal trimethyl phosphate (TMP).

One-dimensional difference NOE experiments were conducted by using a 1–1 H_2O suppression pulse (Hore, 1983). The carrier frequency was shifted 6000 Hz downfield from the H_2O resonance and the delay between 1–1 pulses optimized for H_2O solvent suppression. The FIDs were collected by using 2048 complex data points over a 20 000-Hz sweep width and a 0.7-s repetition delay. The resonance of interest was irradiated for 300 ms by using the decoupler channel. Data collection of the irradiated and control resonances was interleaved every 16 scans for a total of 4096 scans for each of the control and decoupled resonances. The FIDs were subtracted after an exponential line broadening of 3 Hz was applied and Fourier transformed to obtain the NOE difference spectra.

Phase-sensitive two-dimensional NOESY spectra of the GCG 13-mer duplex in H_2O buffer were collected by using a 120-ms mixing time and a 1.0-s repetition delay. A jump-return (90y, t, 90–y) solvent suppression pulse (Plateau & Gueron, 1982) was used for the detection pulse, while the preparation and mixing pulses were replaced by ~70° hard pulses (~7.0 μs). The reduction from a 90° pulse (~9.0 μs) allowed the receiver gain to be increased by at least a factor of 2, significantly increasing the sensitivity (unpublished results). Utilizing a hard pulse for the preparation pulse prevents any offset dependence of excitation in the ω_1 dimension, allowing detection of cross-peaks nearly coincident with the H_2O signal. The carrier frequency was centered on the H_2O signal, and the waiting time, t_w, was optimized for even excitation of the imino and aromatic protons (65 μs). Each of the 256 t_1 increments collected consisted of 1024 complex data points acquired with 256 scans and a sweep width of 10 000 Hz in the t_2 dimension. The free induction decays were apodized with a 90° shifted sine-bell function zeroed at the 1024th point in the t_2 dimension and to the 256th point in the t_1 dimension and with 3-Hz line broadening in both dimensions. Each dimension was baseline corrected with a fifth order polynominal baseline fitting routine after Fourier transformation.

Phase-sensitive two-dimensional nuclear Overhauser effect (NOESY) spectra were collected on the GCG 13-mer duplex in D_2O buffer with a repetition delay of 1.5 s, a sweep width of 10 ppm (5000 Hz at 500 MHz and 4000 Hz at 400 MHz), and a mixing time of 250 ms in D_2O solution. The carrier frequency was positioned on the residual HOD resonance, which was irradiated with the decoupler channel. The data set was collected with 256 t_1 increments by using 1024 complex data points in the t_2 dimension and 32 scans per t_1 increment. The real and imaginary data points were acquired sequentially, and the 512 experiments were merged to yield 256 complex t_1 points (States et al., 1982). The NOESY data sets were Fourier transformed in both dimensions with a 90° shifted sine-bell function zeroed at the 1024th point in the t_2 dimension and at the 256th point in the t_1 dimension.

Magnitude two-dimensional correlated (COSY) experiments on the GCG 13-mer duplex in D_2O were recorded with quadrature detection in both dimensions. The data set was collected with 512 t_1 increments and a sweep width of 5000 Hz by using 1024 complex data points in the t_2 dimension. The magnitude COSY data were collected for 32 scans per t_1 increment and a repetition delay of 1.5 s. The data sets were apodized with an unshifted sine-bell function zeroed at the 512th point and Fourier transformed in both dimensions.

A mixing time of 60 ms was used for achieving optimal relay between the sugar H1′ and H3′ protons in the magnitude relay COSY experiment. All other acquisition and processing parameters were similar to those in the magnitude COSY experiment.

The phase-sensitive two-dimensional ^{31}P–^1H heteronuclear correlation experiment of the GCG 13-mer in D_2O buffer at 25 °C utilized a MLEV-17 composite pulse scheme that achieves a net magnetization transfer among protons via a homonuclear Hartmann–Hahn (HOHAHA) type cross-polarization. This net magnetization transfer is then relayed to the ^{31}P atoms via an INEPT sequence (M. Zagorski, unpublished results). The carrier frequency was placed in the center of the 121.5-MHz phosphorus spectrum. The time domain data sets were accumulated over a sweep width of 260 Hz by using 512 data points in the t_2 dimension. A sweep width of 1800 Hz was used in the t_1 dimension. A total of 123 t_1 increments were collected with a 1.0-s repetition delay and 768 scans per increment. Both dimensions were zero filled to 1024 complex data points prior to Fourier transformation. The t_2 dimension was apodized with 20-Hz line broadening, and the t_1 dimension was apodized with a 90° shifted sine-bell function zeroed to the 123rd point and 3-Hz broadening.

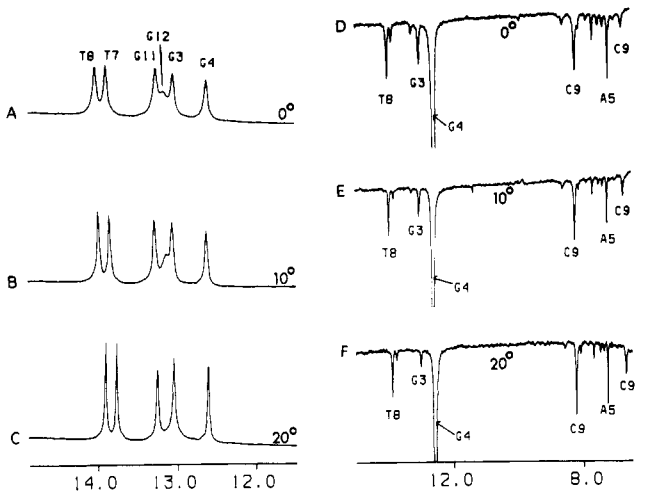

FIGURE 1: Temperature dependence of the exchangeable imino proton spectra (11.6–14.0 ppm) of the GCG 13-mer duplex in 0.1 M NaCl, 10 mM phosphate, and H_2O, pH 6.7 at (A) 0, (B) 10, and (C) 20 °C. One-dimensional NOE difference spectra following 0.3-s saturation of the imino proton of G4 at (D) 0, (E) 10, and (F) 20 °C. The saturated resonance is designated by an arrow.

Scheme I

C1 C2 G3 CX G4 A5 A6 T7 T8 C9 — C10 G11 G12

G12 G11 C10 — C9 T8 T7 A6 A5 G4 CX G3 C2 C1

Data Processing. The one- and two-dimensional data sets were processed by using FTNMR software (D. Hare, unpublished results) on a VAX 11-780 and a MicroVAX II. Streaking in the ω_1 dimension was reduced by using the t_1 noise reduction routine of Klevit et al. (1982) and symmetrized prior to plotting on either a Zeta 822 plotter or a Hewlett-Packard 7475A plotter for analysis, assignment, and publication figures.

RESULTS

The numbering system of the self-complementary GCG 13-mer duplex is outlined in Scheme I. The extra cytidine is designated CX and is flanked by residues G3 and G4.

Exchangeable Proton Assignments. The imino proton spectra (12.0–14.5 ppm) of the GCG 13-mer duplex in 0.1 M NaCl, 10 mM phosphate, and H_2O, pH 6.7 between 0 and 20 °C, are plotted in Figure 1A–C. Six imino protons are detected between 12 and 14 ppm at low temperature.

The exchangeable resonances in the GCG 13-mer have been assigned to specific imino and amino protons in the sequence by analyzing distance connectivities recorded in phase-sensitive NOESY spectra (120-ms mixing time) in H_2O buffer, pH 6.0 at 5 and 20 °C. Distance connectivities linking imino protons (12.0–14.0 ppm) with aromatic base protons and amino protons (7.0–9.0 ppm) within the same base pair and between adjacent base pairs are shown in the expanded contour plot of the GCG 13-mer at 5 °C in Figure 2. Distance connectivities linking imino protons (12.0–14.0 ppm) on adjacent base pairs are shown in expanded symmetrical contour plots of the GCG 13-mer duplex at 5 and 20 °C in Figure 3, parts A and B, respectively. The two downfield imino protons at 13.91 and 13.79 ppm display strong NOEs to adenosine H2 protons (cross-peaks A and E, respectively, Figure 2) characteristic of intra-base-pair NOEs within Watson–Crick A·T base pairs. The assignment of the H2 protons of adenosine are based on NOEs to adjacent sugar H1′ protons in the nonexchangeable proton NOESY experiment described below, allowing the assignment of the 13.91 ppm resonance to the imino proton of T8 and the 13.79 ppm resonance to the imino proton of T7.

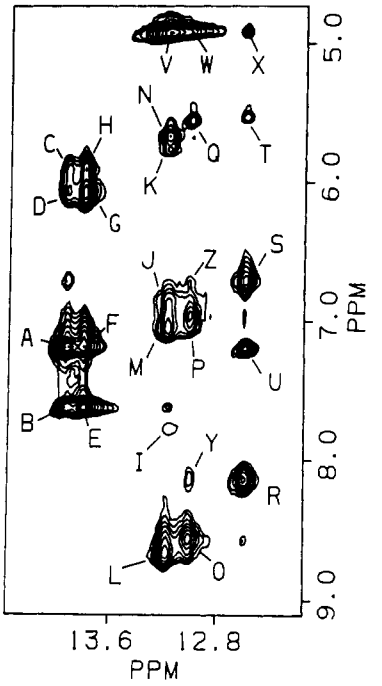

FIGURE 2: Expanded phase-sensitive NOESY contour plot (120-ms mixing time) establishing distance connectivities between the imino protons (12.1–14.1 ppm) and the base and amino protons (4.8–8.8 ppm) in the GCG 13-mer duplex in 0.1 M NaCl, 10 mM phosphate, and H_2O, pH 6.0 at 5 °C. The assignments of the cross-peaks A–Z are as follows: The 13.91 ppm imino proton of T8 exhibits NOE cross-peaks to the H2 protons of A5 (peak A) and A6 (peak B), to the hydrogen-bonded amino protons of A5 and A6 (peak A), and to the exposed amino protons of A5 (peak C) and A6 (peak D). The A5 and A6 amino proton assigments are confirmed by the NOE cross-peak observed between the hydrogen-bonded and exposed amino protons on the same base. The 13.79 ppm imino proton of T7 exhibits NOE cross-peaks to the H2 protons of A6 (peak E) and A5 (peak F), to the hydrogen-bonded amino protons of A6 and A5 (peak F) and to the exposed amino protons of A6 (peak G) and A5 (peak H). The 13.16 ppm imino proton of G12 exhibits NOE cross-peaks to the hydrogen-bonded (peak I) and exposed (peak J) amino protons and the H5 proton (peak K) of C1. The 13.17 ppm imino proton of G11 exhibits NOE cross-peaks to the hydrogen-bonded (peak L) and exposed (peak M) amino protons and the H5 proton (peak N) of C2. The 13.00 ppm imino proton of G3 exhibits NOE cross-peaks to the hydrogen-bonded (peak O) and exposed (peak P) amino protons and the H5 proton (peak Q) of C10, as well as the hydrogen-bonded (peak Y) and exposed (peak Z) amino protons of C9. The 12.59 ppm imino proton of G4 exhibits NOE cross-peaks to the hydrogen-bonded (peak R) and exposed (peak S) amino protons and the H5 proton (peak T) of C9, and to the H2 proton of A5 (peak U). All the cytidine amino proton assignments are confirmed by the observation of NOE cross-peaks between the hydrogen-bonded and exposed amino protons within the same base. Exchange cross-peaks with the solvent H_2O are detected for the imino protons of G11 and G12 (peak V), G3 (peak W), and G4 (peak X).

The three remaining nonterminal imino protons belong to G·C base pairs, and each displays a strong NOE to a hydrogen-bonded cytidine amino proton (cross-peaks L, O, and R, Figure 2) characteristic of Watson–Crick G·C base pairing. The most upfield guanosine imino proton (12.59 ppm) is assigned to G4 since it develops a NOE to the imino proton of T8 (cross-peak A, Figure 3A) and to the H2 proton of A5 (cross-peak U, Figure 2). The guanosine imino proton at 13.00 ppm is assigned to the G3·C10 base pair since it develops a NOE to the imino proton of G4 (cross-peak B, Figure 3A). The imino proton of G3 also develops a NOE to the imino proton of adjacent C2·G11 base pair (cross-peak C, Figure 3A), resulting in the assignment of the 13.17 ppm guanosine imino proton to residue G11. The imino proton at 13.16 ppm is assigned to the terminal G12 residue on the basis of its temperature-

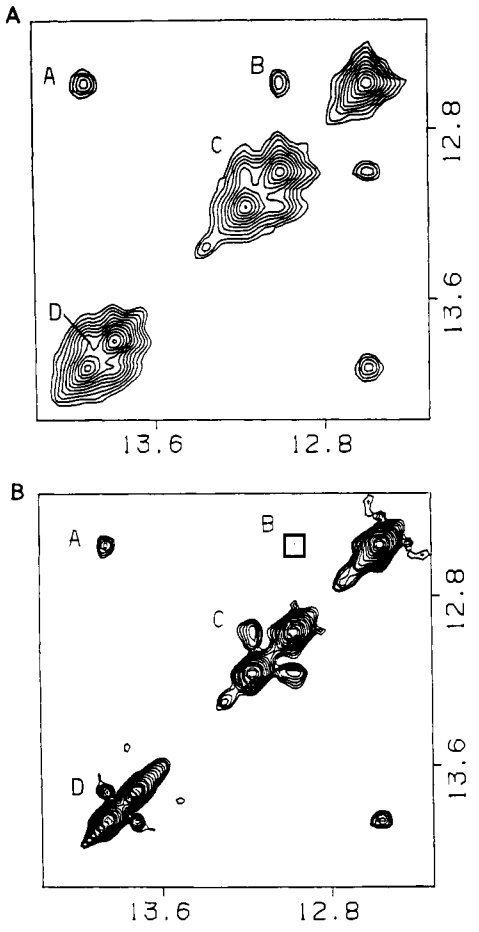

FIGURE 3: Expanded phase-sensitive NOESY contour plots (120-ms mixing time) establishing distance connectivities in the symmetrical imino proton region (12.1–14.1 ppm) in the GCG 13-mer duplex in 0.1 M NaCl, 10 mM phosphate, and H_2O, pH 6.0 at (A) 5 and (B) 20 °C. The assignments of the cross-peaks A–C are as follows: (A) NOE between the imino protons of G4 and T8; (B) NOE between the imino protons of G3 and G4; (C) NOE between the imino protons of G3 and G11; (D) NOE between the imino protons of T7 and T8.

dependent line-width behavior. The imino protons of residues T7 and T8 develop interstrand NOEs to the H2 protons of adjacent residues A5 and A6, respectively (cross-peaks F and B, respectively, Figure 2). The imino protons of T7 and T8 also exhibit NOEs to the hydrogen-bonded and exposed amino protons of adenosine in the same and flanking base pairs (see caption to Figure 2). The complete assignments of the imino, adenosine and cytidine amino, and adenosine H2 protons of the GCG 13-mer, pH 6.0, at 5 °C, are listed in Table I.

Temperature Dependence of Exchangeable Proton NOEs. We detect NOE cross-peaks between exchangeable protons on the G3·C10 and G4·C9 base pairs whose intensities vary as a function of temperature. Thus, the NOE detected between the imino protons of G3 and G4 is stronger at 5 °C (cross-peak B, Figure 3A) than at the higher temperature of 20 °C (box B, Figure 3B). Similarly, the imino proton of G3 exhibits weak NOEs to the hydrogen-bonded (peak Y, Figure 2) and exposed (peak Z, Figure 2) amino protons of C9 at 5 °C, while these NOEs are undetected at the higher temperature of 20 °C.

One-dimensional NOE difference spectra (6–14 ppm) following saturation of the imino proton of G4 in the GCG 13-mer duplex at 0, 10, and 20 °C under identical saturation power and time levels are plotted in parts D, E, and F, respectively, of Figure 1. It can be readily noted that the NOE from the imino proton of G4 is of similar magnitude to the

Table I: Exchangeable Proton Chemical Shifts in the GCG 13-mer Duplex at 5 °C[a]

	chemical shifts (ppm)						
base pair	T-H3	G-H1	C-H4[b]	C-H4[c]	A-H6[d]	A-H6[e]	A-H2
C1·G12		13.16	7.77	6.86			
C2·G11		13.17	8.65	7.04			
G3·C10		13.00	8.57	6.99			
CX							
G4·C9		12.59	8.14	6.71			
A5·T8	13.91				7.20	5.92	7.20
A6·T7	13.79				7.13	6.07	7.63

[a] 0.1 M NaCl, 10 mM phosphate, and H_2O, pH 6.0. [b] Hydrogen-bonded cytidine amino protons. [c] Exposed cytidine amino protons. [d] Hydrogen-bonded adenosine amino protons. [e] Exposed adenosine amino protons.

imino protons of T8 and G3 for the GCG 13-mer duplex at 0 °C (Figure 1D). This ratio changes significantly when the temperature is raised, with the NOE to the imino proton of T8 essentially unchanged while the NOE to the imino proton of G3 exhibits reduced intensity at 20 °C (Figure 1F). These one-dimensional NOEs could not be undertaken above 20 °C due to the onset of exchange broadening of the imino proton of G3 in GCG 13-mer duplex above this temperature.

The imino protons of the GCG 13-mer duplex in 0.1 M NaCl buffer broaden out in a sequential manner with increasing temperature. The imino proton of the terminal C1·G12 pair broadens when the temperature is increased above 15 °C, followed by the imino protons of C2·G11 and G3·C10 pairs that broaden significantly by 40 °C, while the imino protons of the central G4·C9, A5·T8, and A6·T7 pairs broaden above 45 °C.

Nonexchangeable Proton Assignments. The phase-sensitive NOESY spectrum (250-ms mixing time) of the GCG 13-mer duplex in 0.1 M NaCl 10 mM phosphate, pH 6.4, and D_2O has been recorded at 5, 20, 25, and 35 °C.

Expanded regions of the 25 °C NOESY plot establishing distance connectivities from the base protons (7.0–8.2 ppm) to the cytidine H5 and sugar H1′ protons (5.3–6.3 ppm) and sugar H2′,2″ protons (1.2–3.0 ppm) are plotted in parts A and B of Figure 4, respectively.

The majority of the base protons (purine H8 or pyrimidine H6) exhibit NOE cross-peaks to their own and 5′-flanking sugar H1′ protons (Figure 4A), reflecting the directionality of distance connectivities in a right-handed duplex. Deviations from this directionality pattern of base–sugar H1′ NOEs permit identification of structural irregularities in DNA oligonucleotides. Thus, the NOE cross-peak between the H8 of G4 and the H1′ of CX is absent, while that between the H6 of CX and the H1′ of G3 is weak (Figure 4A). The distance connectivities with the exception of the interruption in the CX–G4 step can be traced from C1 to G12 in the GCG 13-mer duplex, and these are outlined in Figure 4A.

We also detect NOE cross-peaks between adjacent base protons in purine H8/pyrimidine H6(3′–5′)pyrimidine H6/CH_3 A6–T7, T7–T8, and T8–C9 steps in the GCG 13-mer duplex characteristic of a right-handed helix. By contrast, no cross-peak is detected between the H8 of G3 and the H5 of CX in the G3–CX step, while severe overlap prevents a search for the possible cross-peak between the H6 of C9 and the H5 of C10 in the C9–C10 step in the GCG 13-mer duplex (Figure 4A).

We detect cross-strand NOEs between the H2 proton of A5 and the H1′ proton of C9 (peak D, Figure 4A) and between the H2 proton of A6 and the H1′ proton of T8 (peak B, Figure 4A) consistent with formation of a right-handed helix in the GCG 13-mer duplex.

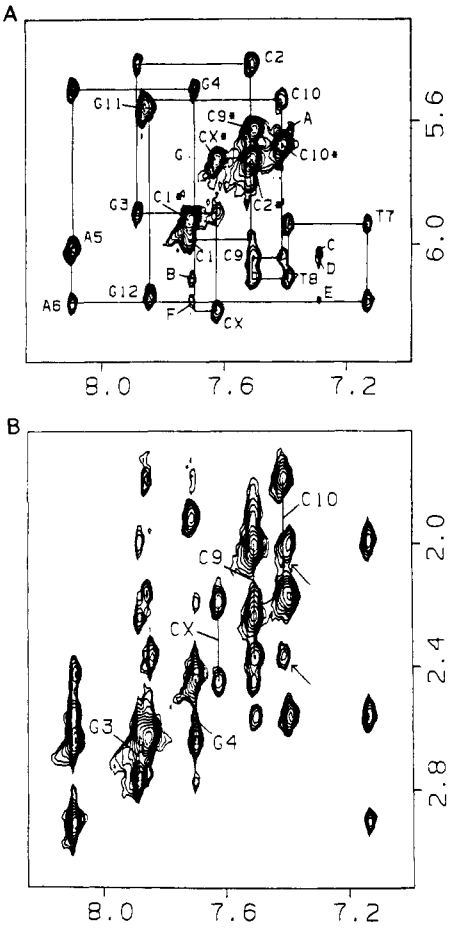

FIGURE 4: Expanded contour plots of the phase-sensitive NOESY spectrum (250-ms mixing time) of the GCG 13-mer duplex, D_2O, 25 °C. (A) Distance connectivities linking the base protons (7.0–8.2 ppm) with the sugar H1′ and cytidine H5 protons (5.3–6.3 ppm). The cross-peaks between H6 and H5 protons of cytidines are designated by asterisks. The NOE cross-peaks A–F are assigned as follows: (A) H6 of T8 and H5 of C9; (B) H2 of A6 and H1′ of T8; (C) H2 of A5 and H1′ of A5; (D) H2 of A5 and H1′ of C9; (E) H2 of A5 and H1′ of A6; (F) H2 of A6 and H1′ of A6. (B) Distance connectivities linking the base protons (7.0–8.2 ppm) with the sugar H2′,2″ protons (1.7–3.0 ppm). The NOEs between the base and their own H2′,2″ protons are labeled for the (G3–CX–G4)·(C9–C10) bulge segment. The arrows indicate NOEs between the H6 proton of C10 and the H2′,2″ protons of C9.

The NOE connectivities between the base protons and their own and 5′-linked sugar H2′,2″ protons are shown in the expanded contour plot in Figure 4B. Lines are drawn linking the sugar H2′ and H2″ protons of G3, CX, G4, C9, and C10 as depicted in Figure 4B. We do not detect NOEs between the H6 of CX and the H2′,2″ protons of G3, while weak NOEs are detected between the H8 proton of G4 and the H2′,2″ protons of CX in the GCG 13-mer duplex. However, NOEs are detected between the H6 proton of C10 and the H2′,2″ protons of C9 (designated by arrows, Figure 4B).

The remainder of the NOESY spectrum of the GCG 13-mer duplex has been analyzed in an analogous manner. We detect NOEs between the H5 proton of C10 and the H2′,2″ protons of C9 but not between the H5 proton of CX and the H2′,2″ protons of G3 in the GCG 13-mer duplex. The nonexchangeable base and sugar ring proton chemical shifts in the GCG 13-mer duplex at 25 °C are listed in Table II.

A NOESY spectrum of the GCG 13-mer duplex in D_2O buffer at 25 °C has also been recorded at a mixing time of 50 ms. These data demonstrate that the NOEs between the H5 and H6 protons of cytidines are much stronger than the NOEs between the base protons and their own sugar H1′

Table II: Nonexchangeable Proton Chemical Shifts in the GCG 13-mer Duplex at 25 °C[a]

	chemical shifts (ppm)								
residue	H8	H2	H6	H5/CH_3	H1′	H2′	H2″	H3′	H4′
C1			7.71	5.92	5.98	1.93	2.45	4.63	4.10
C2			7.51	5.72	5.42	2.01	2.25	4.81	
G3	7.88				5.90	2.77	2.62	5.03	4.34
CX			7.62	5.73	6.21	2.20	2.46	4.71	4.26
G4	7.69				5.50	2.43	2.65	4.83	4.31
A5	8.08	7.28			6.01	2.65	2.92	5.01	4.43
A6	8.09	7.70			6.19	2.57	2.91	5.00	4.47
T7			7.12	1.27	5.93	2.00	2.57	4.83	4.35
T8			7.38	1.54	6.10	2.18	2.57	4.90	4.23
C9			7.50	5.63	6.04	2.03	2.38	4.80	4.21
C10			7.41	5.68	5.53	1.80	2.18	4.81	4.05
G11	7.85				5.56	2.64	2.64	4.93	4.26
G12	7.83				6.17	2.61	2.38	4.66	

[a] 0.1 M NaCl, 10 mM phosphate, and H_2O, pH 6.4.

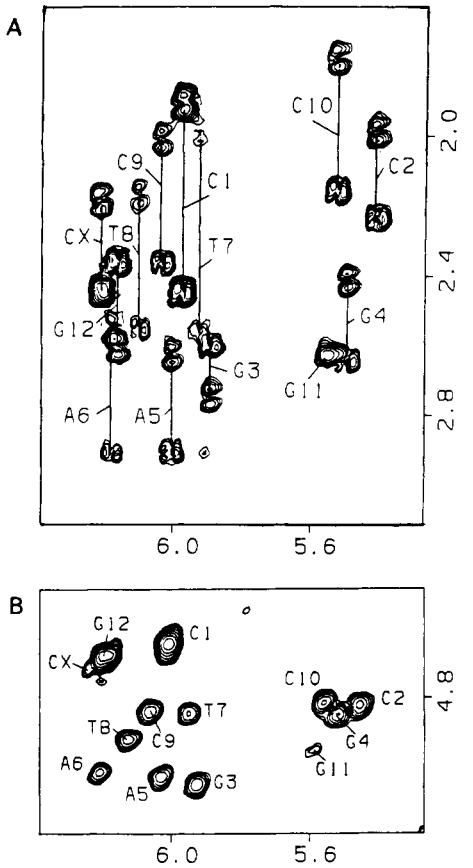

FIGURE 5: (A) Expanded contour plot of the magnitude COSY spectrum of the GCG 13-mer duplex, D_2O buffer, 25 °C, establishing coupling connectivities between the sugar H1′ protons (5.3–6.3 ppm) and the sugar H2′,2″ protons (1.7–3.0 ppm). (B) Expanded contour plot of the magnitude relay COSY spectrum of the GCG 13-mer duplex, D_2O, 25 °C, establishing coupling connectivities between the sugar H1′ protons (5.3–6.3 ppm) and the sugar H3′ protons (4.5–5.2 ppm).

protons for all nucleotides in the GCG 13-mer duplex.

The through bond coupling connectivities have been analyzed by recording magnitude COSY spectra and magnitude relay COSY spectra for the GCG 13-mer duplex in 0.1 M NaCl, 10 mM phosphate, and D_2O at 25 °C. An expanded region of the GCG 13-mer COSY contour plot establishing coupling connectivities between the sugar H1′ protons (5.3–6.3 ppm) and the sugar H2′,2″ protons (1.7–3.0 ppm) is plotted in Figure 5A. The sugar H2′ proton generally resonates to high field of the sugar H2″ proton in deoxyoligonucleotide duplexes. The H1′–H2′ COSY cross-peak pattern is distinctly

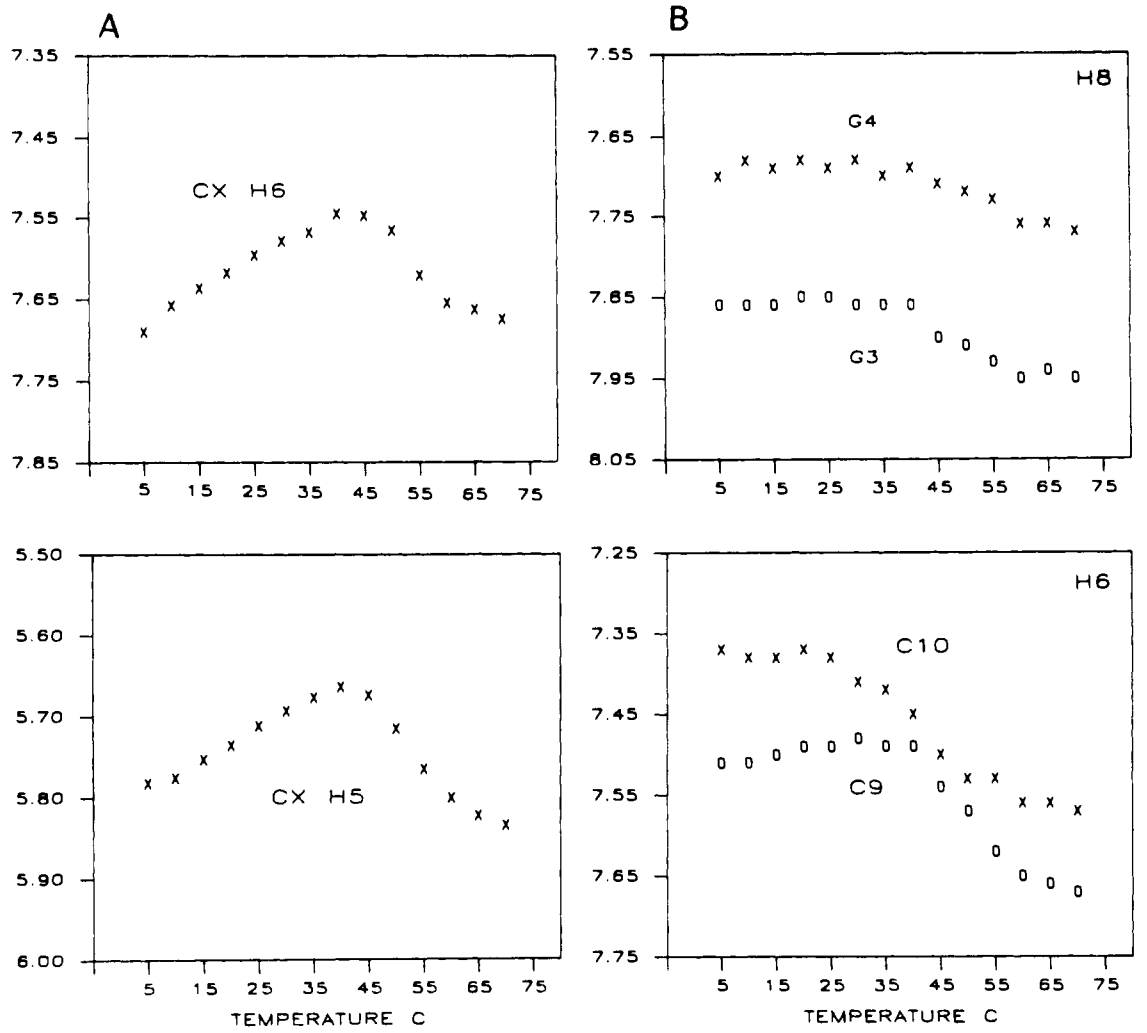

FIGURE 6: Temperature dependence of the nonexchangeable proton chemical shifts of (A) the H5 and H6 protons of CX and (B) the H8 protons of G3 and G4 and the H6 protons of C9 and C10 in the GCG 13-mer duplex in 0.1 M NaCl, 10 mM phosphate, and D_2O, pH 6.7.

different from the H1′–H2″ COSY cross-peak pattern and reflects differences in the three bond coupling constants involving the H2′ and the H2″ protons. The characteristic H1′–H2′ and H1′–H2″ coupling patterns are reversed for residue G3 and for the terminal residue G12 in the GCG 13-mer duplex.

An expanded region of the GCG 13-mer relay COSY contour plot establishing coupling connectivities between the sugar H1′ protons (5.3–6.3 ppm) and the sugar H3′ protons (4.5–5.2 ppm) is plotted in Figure 5B. The relay experiment readily permits coupling connectivities between the H1′ and H3′ protons with the assignments for the GCG 13-mer duplex outlined in Figure 5B. The results of the COSY and relay COSY experiments confirm the nonexchangeable base and sugar ring proton assignments for the GCG 13-mer duplex listed in Table II.

Temperature Dependence of Nonexchangeable Proton Shifts and NOEs. The temperature dependence of the nonexchangeable proton chemical shifts in the GCG 13-mer duplex in 0.1 M NaCl buffer have been recorded between 5 and 70 °C. The chemical shift of the CH_3 protons of T8 and T9 shift upfield in a cooperative transition on proceeding from the strand state (70 °C) to the duplex state (35 °C) with an essentially constant chemical shift in the duplex state between 5 and 35 °C. By contrast, the temperature dependence of the chemical shift of the H6 and H5 protons of CX in the GCG 13-mer exhibits atypical behavior (Figure 6A) with a noncooperative temperature-dependent transition between 5 and 35 °C. The H6 and H5 proton chemical shifts of CX at 5 °C in the GCG 13-mer duplex are characteristic of single-strand values and shift upfield when the temperature is raised to 35 °C (Figure 6A). We have also monitored the remaining base protons in the (G3-CX-G4)·(C9-C10) bulge site as a function of temperature in the GCG 13-mer duplex. The H8 protons of G3 and G4 and the H6 protons of C9 and C10 exhibit essentially temperature-independent chemical shifts between 5 and 40 °C.

The expanded NOESY contour plots of the symmetrical 7.1–8.2 ppm base proton region of the GCG 13-mer duplex in D_2O buffer at 5 and 35 °C are compared in parts A and B, respectively, of Figure 7. The cross-peak assignments are listed in the caption to Figure 7. We note that the NOE cross-peaks between the H8 protons of G3 and G4 (cross-peak A) and between the H8 protons of G4 and A5 (cross-peak B) detected at 5 °C (Figure 7A) are absent at 35 °C (Figure 7B) in the GCG 13-mer duplex.

The expanded NOESY contour plots linking the base protons (7.0–8.2 ppm) with the sugar H1′ protons (5.3–6.3 ppm) of the GCG 13-mer duplex in D_2O buffer at 5 and 35 °C are compared in parts A and B, respectively, of Figure 8. There is less overlap of cross-peaks for the narrow resonances recorded at 35 °C (Figure 8B) than for the broad resonances recorded at 5 °C (Figure 8A).

The base to sugar H1′ distance connectivities can be traced in the 35 °C contour plot for the G3–CX–G4 and C9–C10 steps except for the absence of an NOE between the H8 of

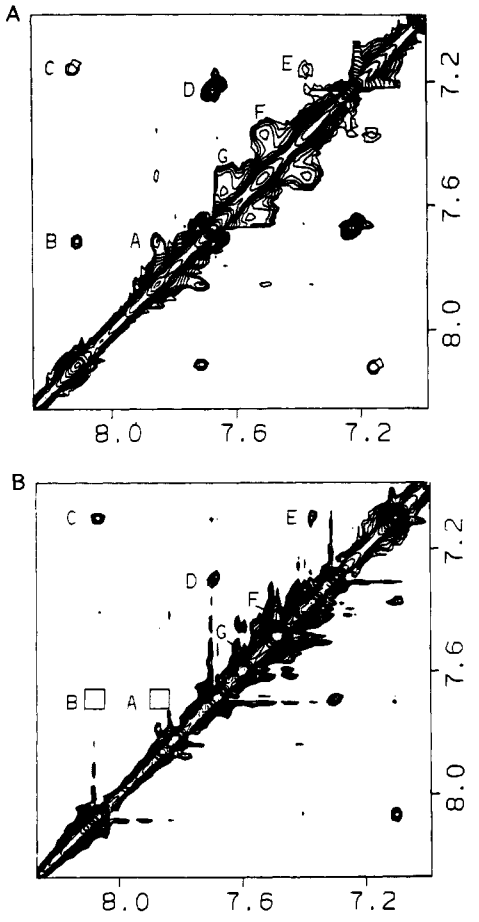

FIGURE 7: Expanded contour plots of the phase-sensitive NOESY spectra (250-ms mixing time) of the GCG 13-mer duplex, D_2O buffer at (A) 5 and (B) 35 °C. The NOE cross-peaks A–G are assigned as follows: (A) H8 of G3 and H8 of G4; (B) H8 of G4 and H8 of A5; (C) H8 of A6 and H6 of T7; (D) H2 of A5 and H2 of A6; (E) H6 of T7 and H6 of T8; (F) H6 of C9 and H6 of C10; (G) H6 of C1 and H6 of C2.

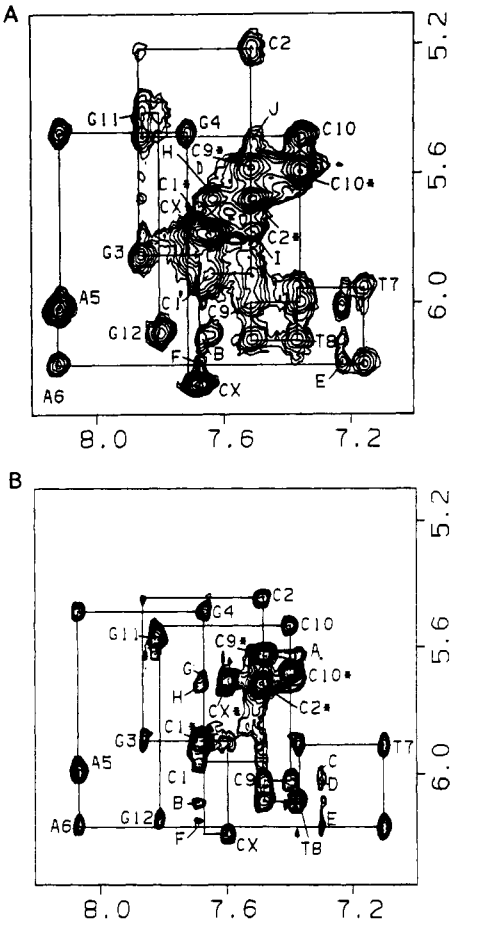

FIGURE 8: Expanded contour plots of the phase-sensitive NOESY spectra (250-ms mixing time) of the GCG 13-mer duplex, D_2O buffer at (A) 5 and (B) 35 °C. The NOE cross-peaks A–F have been assigned in the caption to Figure 4A.

G4 and the H1′ of CX. Further, a pyrimidine H5–purine H8 base to base NOE is detected for the CX–G4 step (cross-peak G, Figure 8B) but not for the G3–CX step. It should also be noted that the H1′ proton of C2 shifts downfield when the temperature of the GCG 13-mer duplex is raised from 5 (Figure 8A) to 35 °C (Figure 8B).

Phosphorus Assignments. The phosphorus resonances are dispersed between 3.7 and 4.5 ppm in the proton Waltz decoupled (Shaka et al., 1983) phosphorus spectrum of the GCG 13-mer duplex in 0.1 M NaCl, 10 mM phosphate, and D_2O at 25 °C. Each phosphorus has the potential to develop direct and relayed couplings to the H3′, H4′, and H2′,2″ protons of the O3′-linked sugar and to the H4′ and H5′,5″ protons of the O5′-linked sugar in the heteronuclear phosphorus (observe) proton relay COSY experiment (Figure 9A) (M. Zagorski, unpublished results). Each phosphorus resonance was assigned through correlation to the assigned sugar H3′ protons, and the ambiguities were resolved by analyzing the relay cross-peaks to the H4′ and the H2′,2″ protons. This is demonstrated in the slice recorded through the most downfield phosphorus resonance at 3.68 ppm as shown in Figure 9B. The phosphorus resonance assignments in the GCG 13-mer duplex at 25 °C are listed in Table III.

Temperature Dependence of Phosphorus Spectra. The proton-decoupled phosphorus spectra of the GCG 13-mer duplex between 10 and 30 °C are plotted in Figure 10. The G3pCX phosphorus resonance shifts downfield when the temperature is raised from 10 to 30 °C (Figure 10).

Table III: Proton–Phosphorus Chemical Shift Correlations: ^{31}P Phosphodiester Resonance Assignments in GCG 13-mer at 25 °C

	chemical shifts (ppm)					
phosphate	P	3′-H3′[a]	3′-H4′[a]	3′-H2′,2″[a]	5′-H4′[b]	5′-H5′,5″[b,c]
C1–C2	−4.04	4.63		1.91, 2.48		4.04
C2–G3	−3.68	4.80		2.00, 2.24	4.33	4.03
G3–CX	−3.94	5.03		2.61, 2.76	4.13?	
CX–G4	−4.19	4.71		2.19, 2.43		4.06
G4–A5	−4.32	4.83			4.43	
A5–A6	−4.40	5.01	4.47			
A6–T7	−4.40	5.01			4.47	
T7–T8	−4.45	4.83			4.23	
T8–C9	−4.37	4.90	4.21			
C9–C10	−4.07	4.79	4.26			
C10–G11	−4.19	4.81			4.24	
G11–G12	−3.86	4.94	4.23			

[a] O3′-linked sugar proton correlations. [b] O5′-linked sugar proton correlations. [c] H5′,H5″ protons assigned solely on the observed ^{31}P correlation.

Discussion

Base Pairing. Six imino protons have been detected for the self-complementary GCG 13-mer duplex in H_2O solution (Figure 1A) with NOEs detected between the thymidine imino protons and adenosine H2 protons within A·T base pairs and between guanosine imino protons and cytidine amino protons within G·C base pairs (Figure 2). These results establish that all base pairs including G3·C10 and G4·C9 flanking the extra cytidine CX are of the Watson–Crick type in the GCG 13-mer duplex. The sequential broadening of the imino protons from the ends of the duplex with increasing temperature demonstrates that the central d(G4-A5-A6-T7-T8-C9) hexanucleo-

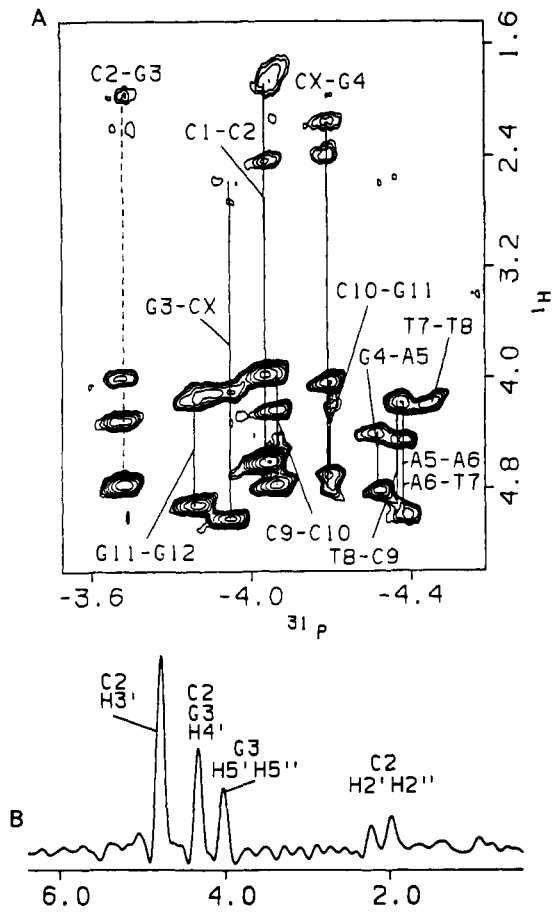

FIGURE 9: (A) Two-dimensional heteronuclear phosphorus (observe) proton relay COSY contour plot of the GCG 13-mer duplex, D_2O at 25 °C. Only positive contours are plotted in the interest of clarity. (B) Slice recorded through the positive contour levels of the 3.68 ppm ^{31}P resonance establishing direct and relay connectivities to the sugar protons in both directions.

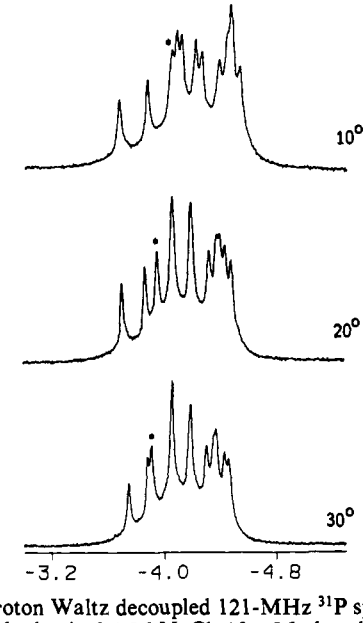

FIGURE 10: Proton Waltz decoupled 121-MHz ^{31}P spectrum of the GCG 13-mer duplex in 0.1 M NaCl, 10 mM phosphate, and D_2O, at 10, 20, and 30 °C. The internucleotide phosphate between G3 and CX (resonance marked with an asterisk) exhibits a temperature-dependent phosphorus chemical shift.

tide core of the duplex is quite stable. The imino protons of the G·C base pairs that flank the extra cytidine CX site exhibit different stabilities, with G4·C9 more stable than G3·C10 in the GCG 13-mer duplex. The detection of NOEs between exchangeable imino protons on adjacent base pairs (cross-peaks A–D, Figure 3) as well as between exchangeable imino and nonexchangeable adenosine H2 and amino protons on adjacent base pairs (Figure 2) is consistent with stacking of the Watson–Crick base pairs along the length of the helix.

Helix Handedness and Type. The observed directionality of the cross-peaks in the NOESY contour plot of the GCG 13-mer duplex in D_2O at 25 °C reflect the handedness of the helix and the glycosidic torsion angles at individual nucleotides along the duplex. The base protons exhibit NOEs to their own and 5′-flanking sugar H1′, H3′, and H2′,2″ protons (Figure 4) consistent with formation of a right-handed helix. The base to sugar H1′ NOE cross-peaks are much weaker than the H5 to H6 cytidine NOE cross-peaks (fixed 2.45-Å separation) at short mixing times, consistent with all nucleotides including CX adopting anti glycosidic torsion angles along the length of the GCG 13-mer duplex.

The formation of a right-handed helix for the GCG 13-mer duplex in aqueous solution is reflected in the observed directionality of the cross-strand NOEs between thymidine imino and adenosine H2 protons on adjacent base pairs (Figure 2), the cross-strand NOEs between adenosine H2 and sugar H1′ protons on adjacent base pairs (Figure 4A), and the same-strand NOEs between adjacent base protons in A6–T7, T7–T8, and T8–C9 steps (Figure 4A).

Helix Interruption Site. The extra cytidine CX results in the formation of a pyrimidine bulge defect in the GCG 13-mer duplex. The consequences of this helix interruption are manifested in the perturbed cross-peak patterns for the (G3–CX–G4)·(C9–C10) segment in the NOESY spectrum of the GCG 13-mer duplex at 25 °C. Specifically, the NOE cross-peaks between the H8 of G4 and the sugar H1′, H2′,2″, and H3′ protons of the 5′-flanking CX and the NOE cross-peaks between the H6 of CX and the sugar H1′,H2′,2″, and H3′ protons of the 5′-flanking G3 are either weak or absent (Figure 4). Similar, NOE cross-peaks are absent between the H5 of CX and the H2′,2″ protons of 5′-flanking G3. By contrast, NOE cross-peaks are detected between either the H6 or H5 of C10 and the H2′,2″ protons of 5′-flanking C9 in the GCG 13-mer duplex (Figure 4B). We also note that the H2″ protons are upfield of their H2′ protons for residue G3 and the terminal residue G12, which is the reverse pattern from what is observed for the remaining sugar H2′,H2″ protons in the COSY contour plot of the GCG 13-mer duplex (Figure 5A).

The most downfield shifted phosphorus resonance in the GCG 13-mer duplex has been assigned to the C2pG3 internucleotide linkage (Figure 9). Thus, the conformational perturbation in the backbone extends beyond the extra cytidine bulge site in the GCG 13-mer duplex and is in agreement with a related observation for an extra adenosine bulge site (Roy et al., 1987).

These results establish that the major perturbation at the extra cytidine bulge site is detected primarily on the (G3–CX–G4) segment centered about the CX residue as compared to the (C9–C10) segment on the partner strand opposite the CX residue for the GCG 13-mer duplex at 25 °C.

Temperature-Dependent Conformational Transition. This NMR study has established a novel structural transition between two conformations of the extra cytidine CX residue in the GCG 13-mer duplex as a function of temperature in the premelting transition region. This transition is most readily monitored at the nonexchangeable proton chemical shifts of the H6 and H5 protons of CX, which shift upfield by ap-

proximately 0.15 ppm between 5 and 35 °C (Figure 6A). This transition can also be followed at the phosphodiester backbone as monitored by the G3pCX phosphate, which shifts 0.2 ppm downfield when the temperature is raised from 10 to 30 °C (Figure 10). Such a premelting conformational transition has not been detected in previous NMR studies of cytidine containing bulge sites (Morden et al., 1983; Woodson & Crothers, 1987) and thymidine containing bulge sites (van den Hoogen et al., 1988a) in deoxyoligonucleotide duplexes.

Looped Out Extra Cytidine at Low Temperature. The proton chemical shift and NOE parameters for the GCG 13-mer duplex demonstrate that the extra cytidine CX is predominantly looped out of the helix at low temperature. Specifically, the H6 and H5 proton chemical shifts of CX at low temperature (5 °C) correspond closely to the high-temperature (70 °C) unstacked strand values for the GCG 13-mer duplex (Figure 6A). This conclusion receives support from the demonstration that the H5 and H6 proton chemical shifts at low and high temperatures are very similar for a looped out uridine in the center of a ribooligonucleotide duplex (van den Hoogen et al., 1988b).

Several lines of evidence establish that the G3·C10 and G4·C9 base pairs stack on each other in the GCG 13-mer duplex at low temperature. The observed NOE between the H8 protons of G3 and G4 (cross-peak A, Figure 7A) is consistent with a looped out CX at the G3–CX–G4 step in the GCG 13-mer duplex in D_2O buffer at 5 °C. Further, an NOE is detected between the imino protons of G3·C10 and G4·C9 (cross-peak B, Figure 3A) in the NOESY spectrum of the GCG 13-mer duplex in H_2O buffer at 5 °C. This result is confirmed in the corresponding one-dimensional NOE experiment where the imino proton of G4 in the G4·C9 base pair exhibits NOEs of similar magnitude to those of the imino protons of G3 and T8 of the G3·C10 and A5·T8 base pairs in the GCG 13-mer duplex in H_2O at 0 °C (Figure 1D). These results demonstrate that the G3·C10 and G4·C9 base pairs are stacked on each other as a consequence of CX looping out of the GCG 13-mer duplex at low temperature. This conclusion reinforces an earlier demonstration that an extra cytidine flanked by adenosines loops out of the center of a complementary deoxyoligonucleotide duplex (Morden et al., 1983).

Stacked Extra Cytidine at Elevated Temperatures. The proton chemical shift and NOE data demonstrate that the conformational equilibrium shifts from a looped out to a stacked extra cytidine with increasing temperature at the bulge site in the GCG 13-mer duplex. Specifically, the H6 and H5 protons of CX shift to high field when the temperature is raised from 5 to 40 °C in the premelting transition region (Figure 6A), consitent with the stacking of the CX between base pairs at elevated temperatures. This conclusion receives support from the recent results that the H6 and CH_3 shift ~0.25 ppm to high field on formation of a stacked thymidine in the center of a deoxyoligonucleotide duplex (van den Hoogen et al., 1988a).

The stacking of the extra cytidine CX into the helix would result in this pyrimidine acting as a spacer between the G3·C10 and G4·C9 base pairs in the GCG 13-mer duplex. This conclusion is supported by the observation that the one-dimensional NOEs between the G3 and G4 imino protons of the G3·C10 and G4·C9 base pairs decrease in intensity relative to the NOE between the G4 and T8 imino protons of the G4·C9 and A5·T8 base pairs in the GCG 13-mer duplex when the temperature is raised from 0 to 20 °C (Figure 1D–F). The same result is detected in the two-dimensional NOESY spectra, where the cross-peak between the imino protons of G3 and G4 (peak B, Figure 3) decreases in intensity when the temperature is raised from 5 to 20 °C in H_2O buffer while the cross-peak between the H8 protons of G3 and G4 (peak A, Figure 7) disappears when the temperature is raised from 5 to 35 °C in D_2O buffer.

The absence of NOEs between the H8 of G4 and the H1′ of CX and between the H8 of G3 and the H5 of CX at the G3–CX–G4 segment for a stacked CX in the GCG 13-mer duplex at 35 °C are paralleled by the absence of the corresponding NOEs at the stacked thymidine site in the extra thymidine containing deoxyoligonucleotide duplex (van den Hoogen et al., 1988a). We do detect an NOE in an overlapping region between the H5 of the stacked CX residue and the H8 of G4 (cross-peak G, Figure 8B) in the CX–G4 step in the GCG 13-mer duplex at 35 °C.

Perturbations Associated with the Looped Out–Stacked Transition. The chemical shift and NOE perturbations associated with the transition from looped out (low temperature) to stacked (elevated temperature) states for the extra cytidine CX in the GCG 13-mer duplex are summarized below. We shall stress both the detection and absence of changes associated with the transition in the (G3–CX–G4)·(C9–C10) segment of the GCG 13-mer duplex.

The chemical shift changes of the H6 and H5 protons of CX between 5 and 45 °C (Figure 6A) clearly demonstrate a temperature-dependent conformational transition in the GCG 13-mer duplex. By contrast, the chemical shifts of the H8 and H6 protons of the G4·C9 and G3·C10 base pairs flanking the bulge site (Figure 6B) appear to be insensitive to the temperature-dependent looped out–stacking equilibrium. This insensitivity is surprising and must reflect compensating ring current contributions between the CX looped out state where the G3·C10 and G4·C9 base pairs stack on each other and the CX stacked state where each of these base pairs stack with the CX residue. The temperature-dependent conformational transition of the CX residue has also been monitored by the observed downfield shift of the G3pCX phosphate when the temperature is raised from 0 to 30 °C (Figure 10).

The chemical shift changes between the looped out and stacked CX states in the GCG 13-mer duplex are not solely restricted to the (G3–CX–G4)·(C9–C10) segment centered about the bulge site. Thus, the H1′ proton of C2 shifts downfield by 0.25 ppm when the temperature of the GCG 13-mer duplex is raised from 5 (Figure 8A) to 35 °C (Figure 8B).

The looped out to stacked CX transition in the GCG 13-mer duplex has been monitored by changes in proton NOE patterns centered about the (G3–CX–G4)·(C9–C10) bulge site. Thus, NOEs detected between the exchangeable imino protons of G3 and G4 at 0 °C become weaker when the temperature is raised to 20 °C (Figures 1 and 3) in the GCG 13-mer duplex in H_2O buffer. Further, the NOE detected between the H8 proton of G3 and G4 at 5 °C (cross-peak A, Figure 7A) is not detected when the temperature is raised to 35 °C (box A, Figure 7B) in the GCG 13-mer duplex in D_2O buffer. These patterns are consistent with the G4·C9 and G3·C10 base pairs stacked on each other when the CX is looped out of the helix at low temperature, while these base pairs are separated by the inserted CX when this base stacks into the duplex at elevated temperature.

The looped out state is also defined by an unusual NOE between the H6 proton of C9 and the H1′ proton of C10 (cross-peak J, Figure 8A) in the C9–C10 step, which is absent in the stacked state (Figure 8B) of the GCG 13-mer duplex.

Further, the stacked state is characterized by an unusual NOE between the H8 proton of G4 and the H5 proton of CX (cross-peak G, Figure 8B) in the CX–G4 step in the GCG 13-mer duplex. Finally, NOE perturbations associated with the transition are also detected outside the (G3–CX–G4)·(C9–C10) bulge site since the NOE detected between the H8 protons of G4 and A5 at 5 °C (cross-peak B, Figure 7A) is absent at 35 °C (box B, Figure 7B) in the NOESY spectrum of the GCG 13-mer duplex in D_2O buffer.

We are currently unable to define the conformational details of either the looped out or stacked states of the GCG 13-mer duplex. The observed conformational equilibrium between these states rules out application of structure reconstruction algorithms to analyze the NOE-based distance constraints as recently applied to extra purine bulge sites in DNA helices (Hare et al., 1986; Woodson & Crothers, 1988). There are published molecular models available for extra thymidine stacked into a DNA oligonucleotide (van den Hoogen et al., 1988a) and an extra uridine looped out in an identical RNA oligonucleotide (van den Hoogen et al., 1988b). These latter models represent energy-minimized structures based on assumed starting conformations and as such suffer from operator bias as well as the absence of input distance constraints that could aid in the differentiation of different families of conformations.

Conclusion

Bulge sites have been implicated as hotspots for frame-shift mutation. An understanding of the conformation of the extra base may provide insights regarding the mechanism of frame-shift mutation and the repair of bulge sites. This NMR study has established that a duplex containing an extra cytidine flanked by guanosines exhibits a temperature-dependent conformational equilibrium in aqueous solution. The extra cytidine is predominantly looped out into solution with stacking of the flanking G·C base pairs on each other at 0 °C, while the extra cytidine is predominantly stacked into the duplex at 35 °C. This contrasts with earlier results on deoxyoligonucleotide duplexes that demonstrated that an extra cytidine in a A-CX-A segment loops out into solution (Morden et al., 1983), while an extra thymidine in a G-TX-G segment stacks into the helix (van den Hoogen et al., 1988a).

The temperature-dependent conformational equilibrium between looped out (low temperature) and stacked (elevated temperature) states of CX in the (G3–CX–G4)·(C9–C10) segment of the GCG 13-mer duplex was unexpected and may reflect the importance of hydrophobic contributions to the stability of the bulge site. Hydrophobic interactions, which are believed to be entropically driven and are thought to contribute to base stacking of DNA in solution (Saenger, 1984), increase their contribution to the free energy of the system as the temperature is raised. This may account for the novel observation that CX is more stable when inserted into rather than looped out of the GCG 13-mer helix at elevated temperature.

References

De Boer, J. G., & Ripley, L. S. (1984) *Proc. Natl. Acad. Sci. U.S.A. 81*, 5528–5531.

Evans, D. H., & Morgan, A. R. (1982) *J. Mol. Biol. 160*, 117–122.

Evans, D. H., & Morgan, A. R. (1986) *Nucleic Acids Res. 14*, 4267–4280.

Hare, D. R., Wemmer, D. E., Chou, S. H., Drobny, G., & Reid, B. R. (1983) *J. Mol. Biol. 171*, 319–336.

Hare, D., Shapiro, L., & Patel, D. J. (1986) *Biochemistry 25*, 7456–7464.

Hore, P. J. (1983) *J. Magn. Reson. 55*, 283–300.

Klevit, R. E. (1985) *J. Magn. Reson. 62*, 551–555.

Li, B. F., Reese, C. B., & Swann, P. F. (1987) *Biochemistry 26*, 1086–1093.

Lomant, A. J., & Fresco, J. R. (1973) *J. Mol. Biol. 77*, 345–354.

Morden, K. M., Chu, Y. G., Martin, F. H., & Tinoco, I., Jr. (1983) *Biochemistry 22*, 5557–5563.

Nelson, J. W., & Tinoco, I., Jr. (1985) *Biochemistry 24*, 6416–6421.

Patel, D. J., Kozlowski, S. A., Marky, L. A., Rice, J. A., Broka, C., Itakura, K., & Breslauer, K. J. (1982) *Biochemistry 21*, 445–451.

Plateau, P., & Gueron, M. (1982) *J. Am. Chem. Soc. 104*, 7310–7311.

Reese, C. B., & Zard, L. (1981) *Nucleic Acids Res. 9*, 4611.

Ripley, L. S. (1982) *Proc. Natl. Acad. Sci. U.S.A. 79*, 4128–4132.

Roy, S., Sklenar, V., Appella, E., & Cohen, J. S. (1987) *Biopolymers 26*, 2041–2052.

Saenger, W. (1984) in *Principles of Nucleic Acid Structure*, pp 134–140, Springer, New York.

Shaka, A. J., Keeler, J., Frenkiel, T., & Freeman, R. (1983) *J. Magn. Reson. 52*, 335–338.

States, D. J., Haberkorn, R. A., & Ruben, D. J. (1982) *J. Magn. Reson. 48*, 286–292.

Streisinger, G., Okada, Y., Emrich, J., Newton, J., Tsugita, A., Tzeraghi, E., & Inouye, M. (1966) *Cold Spring Harbor Symp. Quant. Biol. 31*, 77–84.

van den Hoogen, Y. T., van Beuzekom, A. A., van den Elst, H., van der Marel, G. A., van Boom, J. H., & Altona, C. (1988a) *Nucleic Acids Res. 16*, 2971–2986.

van den Hoogen, Y. T., van Beuzekom, A. A., de Vroom, E., van der Marel, G. A., van Boom, J. H., & Altona, C. (1988b) *Nucleic Acids Res. 16*, 5013–5030.

White, S. A., & Draper, D. E. (1987) *Nucleic Acids Res. 15*, 4049–4064.

Williams, L. D., & Goldberg, I. H. (1988) *Biochemistry 27*, 3004–3011.

Woodson, S. A., & Crothers, D. M. (1987) *Biochemistry 26*, 904–912.

Woodson, S. A., & Crothers, D. M. (1988) *Biochemistry 27*, 3130–3141.